Available online at www.sciencedirect.com

SciVerse ScienceDirect

Ceramics International 38 (2012) 3121–3128

CERAMICS INTERNATIONAL

www.elsevier.com/locate/ceramint

Nano-indentation on nickel aluminate spinel and the influence of acid and alkaline attacks on the spinel surface

Yue He, Kaimin Shih *

Department of Civil Engineering, The University of Hong Kong, Pokfulam Road, Hong Kong, Hong Kong Special Administrative Region

Received 2 November 2011; received in revised form 6 December 2011; accepted 6 December 2011
Available online 14 December 2011

Abstract

Nickel aluminate spinel phase was successfully sintered from the thermal reactions between nickel oxide and kaolinite or γ-alumina precursor, to simulate the stabilization mechanism of hazardous metal-bearing waste by ceramic matrix. The product phases were then tested using nano-indentation to obtain their nanohardness and Young's modulus, as a means to evaluate the properties of the product after incorporating the waste material. The results indicate the beneficial effect of forming aluminate spinel phase in the system due to its superior mechanical properties. A higher sintering temperature was found to enhance crystal growth in the spinel phase, together with its nanohardness and modulus. The minimum temperature for fabricating nickel aluminate spinel with a surface property comparable to ceramic materials was found to be 1200 °C, although the initiation of the spinel phase can be achieved at a lower temperature. Nano-indentation experiments performed on the spinel-containing samples leached by strong acid and alkaline solutions reveal the superiority of nickel aluminate spinel in resisting acid and alkaline attack and also suggest a reliable mechanism for hosting hazardous nickel in the crystal structure.

Keywords: D. Spinel; Nano-indentation; Nanohardness; Acidic/alkaline attack

1. Introduction

Hazardous metals are widely known for their toxicity to human health and ecosystems. Many investigations have investigated methods for preventing the release of such environmentally persistent pollutants into soils and aquifers [1–5]. For example, various precipitation processes are commonly used to remove hazardous metals from wastewater streams. However, such processes usually result in a large amount of metal-laden sludge that requires further stabilization before disposal [6–8]. Nickel is a major type of hazardous metal among the pollutants generated by electroplating operations [9–11]. Electroless nickel plating plays an important role in manufacturing industries, especially for the fabrication of corrosion-resistant articles. Wastewater generated from this type of processing can contain nickel concentrations of several thousand ppm or higher [6,12,13]. After undergoing metal extraction procedures for recovery purposes, the resulting sludge is then subject to be solidified/stabilized by cementing or thermal process to immobilize the residual metals prior to landfill disposal [14,15].

In developing a waste-to-resource strategy, a close system of material flow must be sought and the beneficial use of metal-laden sludge has attracted strong interest. Recent studies have revealed a potential mechanism for fixing nickel within the nickel aluminate spinel ($NiAl_2O_4$) structure in ceramic products, by sintering nickel oxide with kaolinite and γ-alumina precursors [16–19]. Alumina (Al_2O_3) is one of the most abundant compositions in earth materials and γ-alumina is the thermodynamically favorable phase at temperatures below 750 °C [20]. Kaolin, consisting chiefly of kaolinite ($Al_2Si_2O_5(OH)_4$), is a common type of clay, and most ceramic raw materials contain high percentages of kaolinite (40–65%) [21]. When sintered at temperatures higher than 1200 °C for 3 h, nickel aluminate spinel is effectively formed by incorporating more than 85% of the nickel in the raw material blended with γ-alumina or kaolinite precursor [17]. For products fabricated from waste materials, the surface properties of the product need to be investigated in detail because the failure of metal mobilization is usually initiated on the surface.

* Corresponding author. Tel.: +852 2859 1973; fax: +852 2559 5337.
E-mail address: kshih@hku.hk (K. Shih).

0272-8842/$36.00
doi:10.1016/j.ceramint.2011.12.013

The effect of surface deterioration, such as under acid or alkaline attack, may be reflected by the mechanical properties of the surface because the structure of the near-surface region may have been extensively re-rearranged. For example, the formation of a new mineral phase, the amorphization or change in the properties of the grain boundary, usually leads to the alteration of the mechanical properties of the solid surface.

The hardness and elastic modulus, two major parameters commonly used for describing the mechanical properties of solids, are usually very high for ceramic materials [22–25]. Therefore, the conventional test for bulk samples is not capable of reflecting the small changes in these two parameters caused by the deterioration of the ceramic surface. In contrast, the surface indentation experiment carried out by a nano-indenter can be used to probe the mechanical properties of the solid surface by measuring the nano-scale penetration depth of the indenter and the applied force [26–30]. Such information is highly valuable for examining the robustness of the ceramic surface after a chemical attack, which is critical for determining whether the hazardous metals have been effectively immobilized.

This study first prepared the samples containing nickel aluminate spinel fabricated from the γ-alumina and kaolinite precursors, and nano-indentation was then employed to measure the hardness and elastic modulus of the sample surfaces. To investigate the influence of chemical attack on the ceramic surface, the surface mechanical properties of samples soaked in an HNO_3 or NaOH aqueous solution (6 M) were also measured to compare the change in surface characteristics. To our knowledge, this is the first work to report the use of nano-indentation to assist the investigation of metal stabilization effects for environmental purpose.

2. Experimental methods

Nickel oxide (NiO), kaolin, and γ-Al_2O_3 were used as the starting materials for fabricating products containing nickel aluminate spinel. NiO powder was purchased from Fisher Scientific, with a measured surface area of 3.6 ± 0.5 m^2/g after degassing by heating at 300 °C with He-gas purging for 3 h. USP-grade acid-washed kaolin powder from Fisher Scientific yielded a BET surface area of 9.0 ± 2.9 m^2/g, and its powder X-ray diffraction (XRD) pattern matched kaolinite (ICDD PDF #78-1996). The diffraction patterns were collected using a Rigaku Geigerfex diffractometer (Rigaku Denki Co. Ltd.) equipped with a Cu X-ray tube operated at 35 kV and 15 mA. Scans were collected by a MDI XRD diffractometer-control and data-acquisition system (Material Data, Inc.) from 10° to 80° 2θ-angle, with a step size of 0.02° and a counting time of 1 s per step. The γ-Al_2O_3 was prepared from HiQ-7223 alumina powder (Alcoa Corporation) with a reported surface area of 228 m^2/g and a particle diameter of 54.8 μm in d_{50}. XRD analysis confirmed that as-received HiQ-7223 alumina was boehmite (AlOOH; ICDD PDF #74-1895), which was transformed into a γ-Al_2O_3 dominant material after heat treatment at 650 °C for 3 h [30,31]. The NiO and the kaolin (or γ-Al_2O_3) precursor was mixed with an Ni:Al molar ratio of 1:2 by ball-milling in a water slurry for 22 h and was then dried at 95 °C overnight. The powder was further homogenized by grinding and was then formed into 13 mm pellets at 125 MPa and sintered at 1140 °C, 1200 °C and 1480 °C for 3 h. The fired ceramic pellets were air-quenched and polished with sub-micrometer diamond-lapping film for electron-microscopy scanning (FEI XL30, USA) and nano-indentation (Hysitron TI900, USA) analyses, or ground into powders for XRD analysis.

The nano-indentation experiment began with the 1480 °C sintered product of NiO + kaolinite (NK1480A), and then compared the result after leaching the same sample in a 6 M HNO_3 solution for 160 min (NK1480B). The NiO + γ-Al_2O_3 raw material was sintered at 1140 °C (NA1140A) to achieve a partial transformation to nickel aluminate spinel, and at 1200 °C (NA1200A) for more complete spinel formation. The nano-indentation was performed on these two γ-Al_2O_3 system samples and their 80 min 50% NaOH-leached samples (NA1140B and NA1200B) to observe the influence of the alkaline environment.

The nano-indentation was carried out using a tribo-indenter with a diamond Berkovich indenter. The indentation load, P (between 0 and 10 mN), and displacement, h, were recorded during each loading–unloading cycle. The contact area between the indenter and the sample could be less than 10^{-12} m^2, and as a result it was possible to identify the properties for specific positions on the sample in the data. A typical load versus indentation-depth curve is illustrated in Fig. 1, and the mechanical properties were derived using the method reported previously [26–28]. During the loading period, the total displacement, h, is regarded as $h = h_s + h_c$, where h_c is the vertical distance along which contact is generated and h_s is the

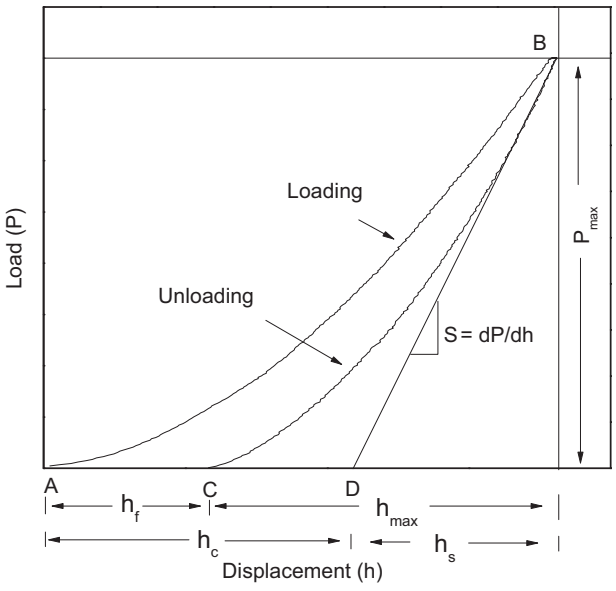

Fig. 1. A schematic representation of load versus indenter displacement data for an indentation experiment. The P_{max} is the peak indentation load; h_{max} is the indenter displacement at peak load; h_f is the final depth of the contact impression after unloading; S is the initial unloading stiffness; h_c is the vertical distance along which contact is generated, and h_s is the displacement of the surface at the perimeter of the contact.

displacement of the surface at the perimeter of the contact. At peak load, the load and displacement are referred to as P_{max} and $h_{max,}$ respectively. Upon unloading, the elastic displacements are recovered, and when the indenter is completely withdrawn the final depth of the residual indenter impression is h_f.

The nanohardness (H) is defined as the mean contact pressure under the condition of the indenter at maximum load (P_{max}):

$$H = \frac{P_{max}}{A_c} \tag{1}$$

where the contact area, A_c, is calculated from an area function using the contact depth (h_c) and the specific shape of the indenter tip as the parameters [26,27]. The contact depth (h_c) is related to the maximum indentation depth (h_{max}) by:

$$h_c = \frac{h_{max} - \varepsilon P_{max}}{S} \tag{2}$$

where S is the contact stiffness and is defined as an increment in the load divided by the resulting increment in displacement without plastic deformation. In our case, the value of ε was adopted as 0.75 for the Berkovich diamond indenter. The slope at maximum load can be calculated from the unloading curve:

$$S = \left(\frac{dP}{dh}\right)_{P=P_{max}} \tag{3}$$

By integrating Eqs. (2) and (3), h_c can be obtained to determine the contact area, A_c, from the area function and to estimate the nanohardness via Eq. (1).

The Young's modulus (E_s) and Poisson's ratio (ν_s) for the specimen can also be obtained from the indentation experiment. The contact stiffness can also be expressed by:

$$E_r = \frac{\pi(S/2)^2}{A_c} \tag{4}$$

where the reduced modulus, E_r, accounts for the fact that the measured elastic displacement includes contributions from both the specimen and the indenter. The reduced modulus is given by:

$$\frac{1}{E_r} = \frac{1-\nu_s^2}{E_s} + \frac{1-\nu_i^2}{E_i} \tag{5}$$

where E_s and ν_s are the elastic modulus and Poisson's ratio for the specimen; E_i and ν_i are the same modules as for the indenter. The ν_s can be defined by the fraction (or percent) of expansion divided by the fraction (or percent) of compression, which is measured during the loading process. Therefore, the value of E_s can be determined by Eq. (5) after obtaining E_r from Eq. (4). In this study, multiple loading–unloading cycles were performed for each specimen in the nano-indentation experiments.

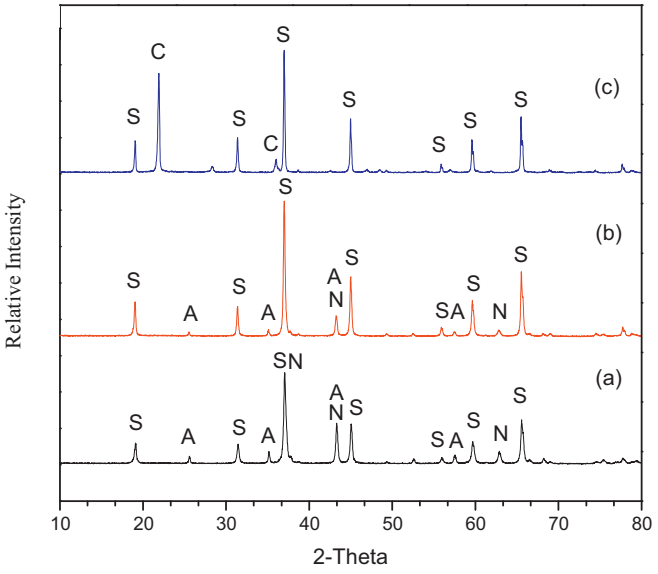

Fig. 2. The XRD results for the 3-h sintered products of (a) NiO + γ-alumina at 1140 °C, (b) NiO + γ-alumina at 1200 °C, and (c) NiO + kaolinite at 1480 °C. "S" represents nickel aluminate spinel ($NiAl_2O_4$, ICDD PDF #78-0552); "N" represents nickel oxide (NiO; ICDD PDF #78-0429); "A" represents corundum (α-Al_2O_3; ICDD PDF #83-2080); and "C" represents cristobalite (SiO_2; ICDD PDF #76-0938).

3. Results and discussion

3.1. Formation of nickel aluminate spinel

Fig. 2 shows the XRD patterns of the products sintered from the NiO + γ-Al_2O_3 and NiO + kaolinite mixtures. The results confirm that Ni was significantly incorporated into the aluminate spinel structure ($NiAl_2O_4$) using both the γ-Al_2O_3 and the kaolinite precursors. With the γ-Al_2O_3 precursor, the incorporation reaction can be expressed as:

$$NiO + Al_2O_3 \rightarrow NiAl_2O_4 \tag{6}$$

Because the sintering temperatures (1140 °C and 1200 °C) for the NiO + γ-Al_2O_3 system were lower than for the NiO + kaolinite system (1480 °C), residues of unreacted nickel oxide and α-Al_2O_3 (a high temperature phase of γ-Al_2O_3) were still observed in the XRD results (Fig. 2a and b). When kaolinite is used as the sintering precursor, the phase transformation of kaolinite under thermal conditions occurs and is known as the kaolinite-to-mullite reaction series [32,33]. During this process, it is usually considered that physically bound water is removed at 105 °C, followed by the decomposition of kaolinite with the loss of chemically bound water and transformation of amorphous metakaolin above 550 °C. At 1000 °C, mullite starts to form with excess amorphous silica, which is converted to cristobalite upon further heating. Therefore, the interaction between NiO and mullite at high temperatures is as follows:

$$3NiO + 3Al_2O_3 \cdot 2SiO_2(\text{mullite}) \rightarrow 3NiAl_2O_4 + 2SiO_2 \tag{7}$$

Fig. 3 shows the scanning electron micrographs of the polished surface of sintered products. Three chemically distinct areas are observable in Fig. 3a (the NiO + γ-Al_2O_3 mixture sintered at

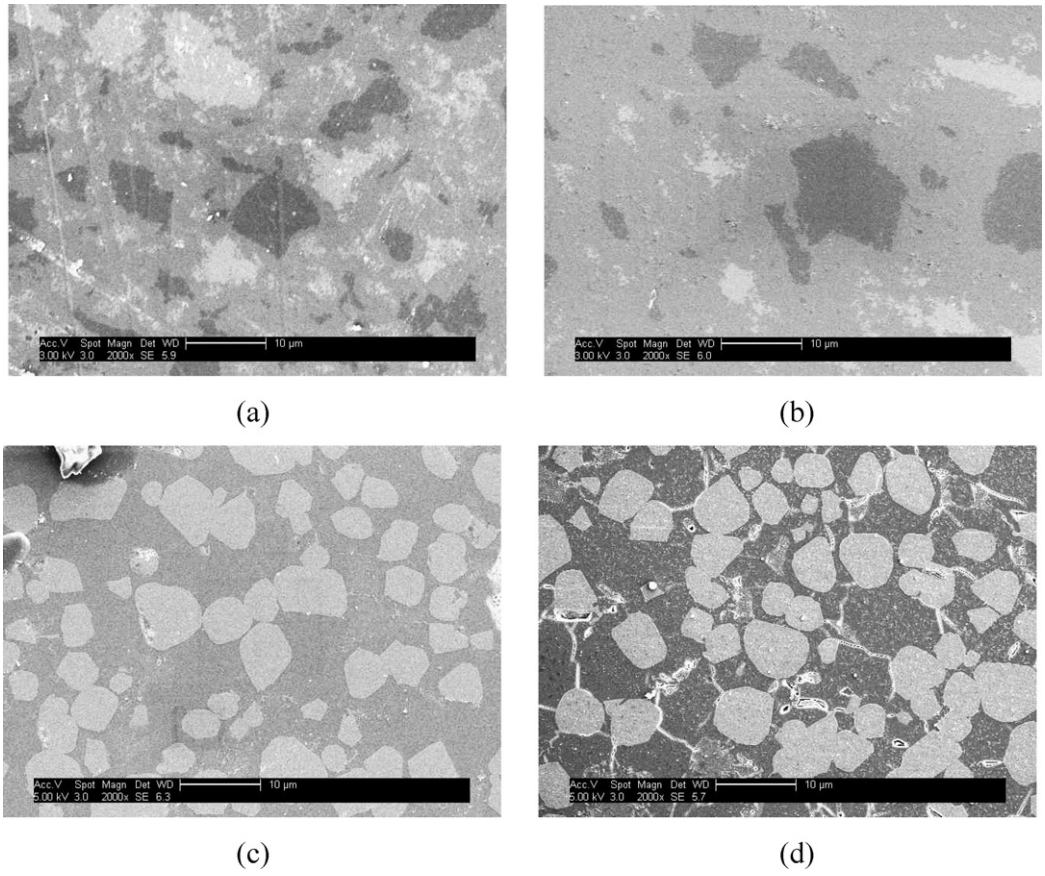

Fig. 3. Scanning electron micrographs of the polished sample surfaces of (a) NiO + γ-Al_2O_3 sintered at 1140 °C (NA1140A); (b) NiO + γ-Al_2O_3 sintered at 1200 °C (NA1200A); (c) NiO + kaolinite sintered at 1480 °C (NK1480A); and (d) NiO + kaolinite sintered at 1480 °C followed by 6 M HNO_3 leaching for 160 min (NK1480B). Samples (a) and (b) show the co-existence of $NiAl_2O_4$, NiO and α-Al_2O_3 phases. The light-colored grains in samples (c) and (d) are enriched by Ni and Al ($NiAl_2O_4$), and the darker matrix shows the enrichment of Si (cristobalite). The Si-matrix is clearly more vulnerable to acid attack than the $NiAl_2O_4$ grains, as reflected in (d).

1140 °C/3 h) and 3b (the NiO + γ-Al_2O_3 mixture sintered at 1200 °C/3 h), which can be identified as NiO, $NiAl_2O_4$, and Al_2O_3 by integrating the results of the XRD and electron dispersive spectroscopy (EDS) equipped with SEM. Fig. 3c shows phase separation when the NiO + kaolinite mixture was sintered at 1480 °C/48 h, and the light-colored grains were indentified as nickel aluminate spinel together with a dark-colored cristobalite matrix. After the sample was subject to acid attack (soaking in 6 M HNO_3 solution for 160 min), the spinel grains were found to remain intact, whereas substantial cracks were found in the cristobalite matrix, as shown in Fig. 3d. This observation clearly reflects the stronger acid resistance of the $NiAl_2O_4$ phase, compared with the cristobalite phase.

3.2. Effects of acid attack on nanohardness and Young's modulus

The nano-indentation experiments were performed on samples sintered from both alumina and kaolinite precursors, and aimed to compare the influence of acid/alkaline attack on the product phases (Table 1). Samples sintered from the kaolinite precursor showed phase separation, therefore a minimum of four nano-indentation experiments were performed for each of these two chemically distinct areas, $NiAl_2O_4$ and SiO_2, identified as nickel aluminate spinel and cristobalite, respectively. The curves of different colors in Fig. 4a represent the multiple loading-unloading cycles performed on the spinel area in sample NK1480A (NiO + kaolinite sintered at 1480 °C), and the nanohardness and modulus values were obtained as 18.1 GPa and 159.1 GPa, respectively. Similar experiments conducted in the cristobalite area resulted in values of 6.2 GPa and 55.0 GPa for nanohardness and modulus, respectively. The wider variation in the load–displacement curves of the spinel area compared with the cristobalite area generally indicates a more consistent surface mechanical property of cristobalite in the sintered products. However, the higher values for nanohardness and modulus in the spinel indicate its superior resistance to permanent plastic and elastic deformations when force is applied to the surface. Because spinel and cristobalite co-exist in the products, the spinel will clearly be a key factor in resisting the deformation of the product surface when subject to external forces. The results also indicate a preferred mechanism for hosting hazardous nickel in the more robust spinel phase.

After leaching the NK1480A sample in a 6 M HNO_3 solution for 160 min, the NK1480B sample was subjected to the nano-indentation experiments, as shown in Fig. 5. Tests on the spinel area (Fig. 5a) showed that the shapes and locations of the load–displacement curves were much more consistent than

Table 1
Nanohardness and Young's modulus of the samples tested in this study.

Source	Sample	Phase	Nanohardness (GPa)	Young's modulus (GPa)
Nickel aluminate spinel sintered from kaolinite precursor	NK1480A: sintered by 1480 °C for 3 h	Spinel	18.1 ± 0.2	159.1 ± 1.8
		Cristobalite	6.2 ± 0.2	55.0 ± 0.7
	NK1480B: NK1480A in 6 M $HNO_{3(aq)}$ for 160 min	Spinel	17.6 ± 0.2	163.8 ± 1.5
		Cristobalite	5.0 ± 0.1	41.6 ± 0.5
Nickel aluminate spinel sintered from γ-alumina precursor	NA1140A: sintered by 1140 °C for 3 h	Spinel	1.0 ± 0.1	1.6 ± 0.2
	NA1140B: NA1140A in 50% $NaOH_{(aq)}$ for 80 min	Spinel	3.2 ± 0.1	95.1 ± 0.7
	NA1200A: sintered by 1200 °C for 3 h	Spinel	4.5 ± 0.1	109.1 ± 1.0
	NA1200B: NA1200A in 50% $NaOH_{(aq)}$ for 80 min	Spinel	7.1 ± 0.2	131.1 ± 1.2

those of the sample before acid leaching. However, the average nanohardness and modulus values (17.6 GPa and 163.8 GPa) obtained from the load–displacement curves were still very close to the average values for the spinel area in the sample before acid leaching. Further comparison of the cristobalite area (Fig. 5b) shows decreases in both the nanohardness and modulus values in the acid-leached sample. These results indicate that although other materials, such as grain boundary substances, may sometimes affect the surface properties of sintered spinel, its intrinsic surface properties are highly robust and consistent after removing surface impurities. However, this is not the case for cristobalite, and the leached cristobalite area produced a weaker surface layer, presumably due to the amorphization of cristobalite after acid attack.

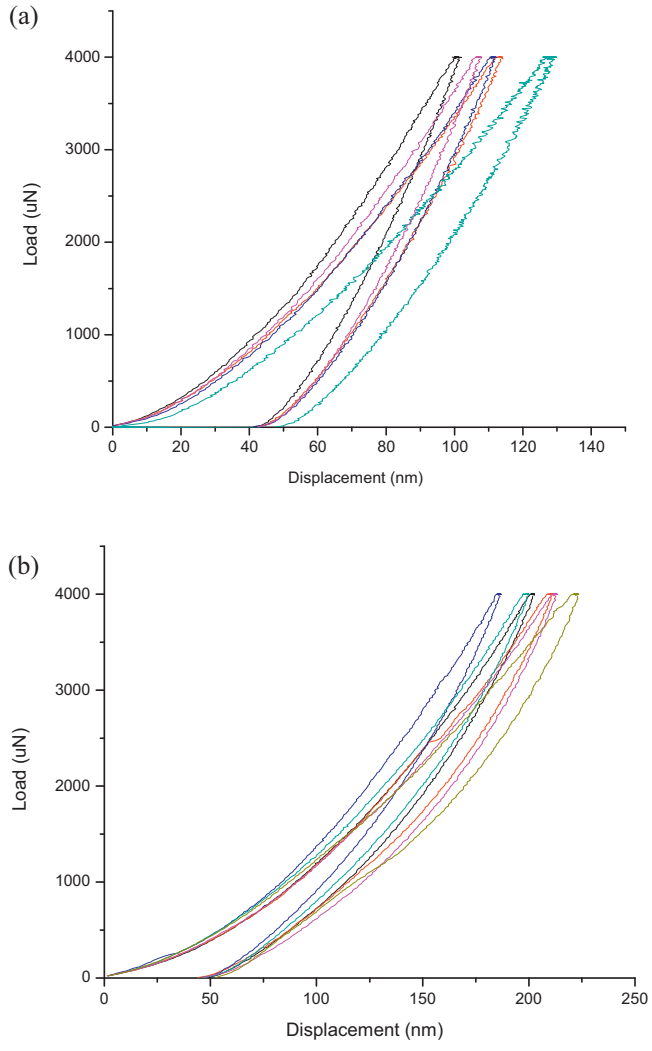

Fig. 4. Nano-indentation load–displacement curves of (a) the spinel phase and (b) the cristobalite phase obtained from the1480 °C/3 h sintered NiO + kaolinite sample (NK1480A).

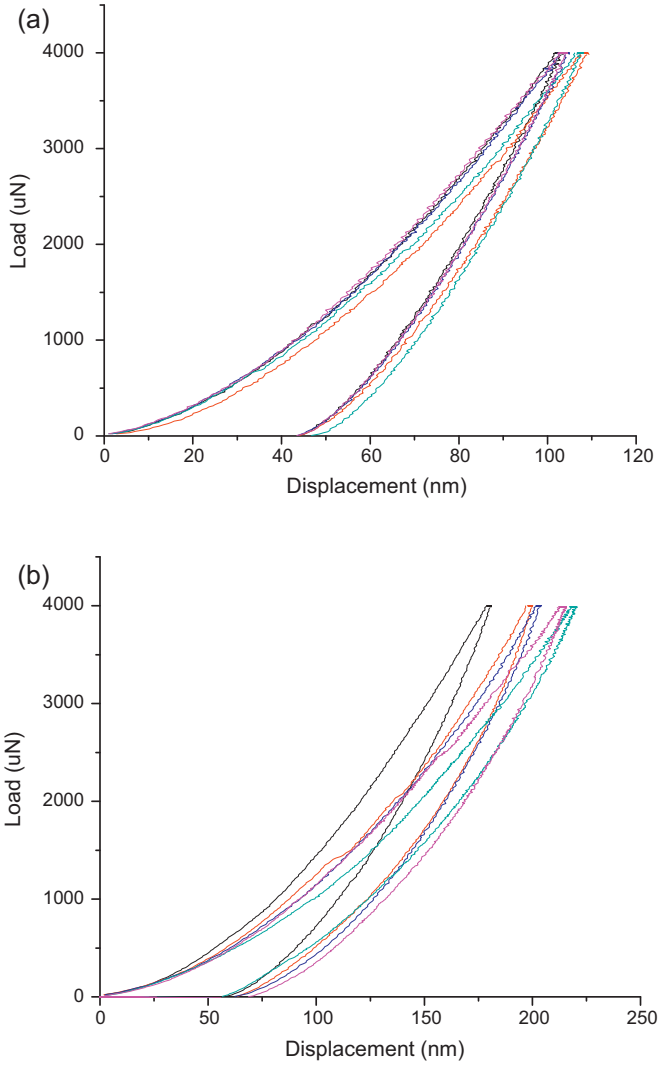

Fig. 5. Nano-indentation load–displacement curves of (a) the spinel phase and (b) the cristobalite phase obtained from the 1480 °C/3 h sintered NiO + kaolinite sample leached by 6 M HNO_3 solution for 160 min (NK1480B).

3.3. Effect of alkaline attack on nanohardness and Young's modulus

Because the nickel aluminate spinel formed at high temperature (1480 °C) was found to be robust in resisting acid attack, further nano-indentation experiments were carried out to observe the performance of the lower-temperature samples under an alkaline environment. The NiO + γ-Al_2O_3 sample sintered at 1140 °C (NA1140A), representing the initial stage of spinel dominance in the sample, was selected to obtain its load–displacement curves, as shown in Fig. 6a. Much deeper displacement under the same loading was observed from the load–displacement curves, and the average nanohardness and modulus values were 1.0 GPa and 1.6 GPa, respectively. This result clearly indicates a product with much weaker surface strength that is highly subject to surface deformation when subjected to external force. This result may be due to the reactant residues among the spinels and/or the low level of crystallinity in the spinel phase generated at this temperature. Because the transformation of very poorly crystalline γ-Al_2O_3 to α-Al_2O_3 is limited by both temperature and kinetics constraints, the unreacted γ-Al_2O_3 may still exist in the areas where the spinel structures are newly formed. It is also likely that the weak structure of the spinel phase has poor connectivity among its small crystals due to the low sintering temperature. Further leaching the NA1140A sample with 50% NaOH solution for 80 min (NA1140B) increased the average nanohardness and modulus values to 3.2 GPa and 95.1 GPa, respectively. This result may further confirm the role of intergranular substances in dominating the mechanical property of products sintered at insufficient temperatures. Although the overall nanohardness and modulus values increased after alkaline leaching, a wider range in the load–displacement curves was obtained, which may also reflect the heterogeneous nature of products with incomplete sintering reaction (Fig. 6b).

A higher sintering temperature is expected to improve the mechanical strength and metal incorporation reaction.

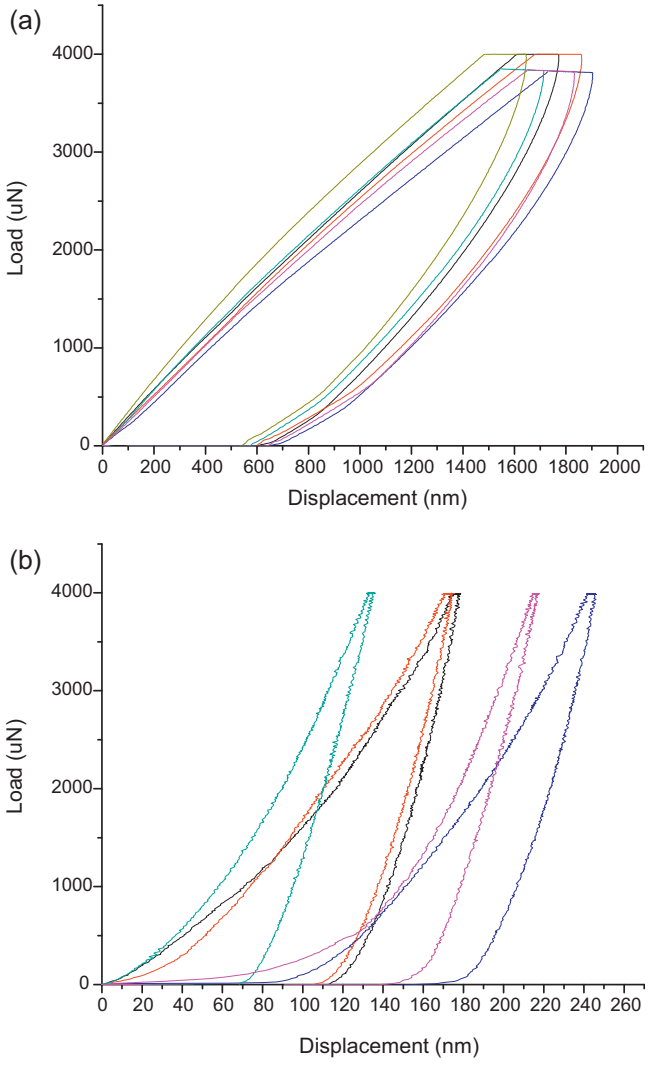

Fig. 6. Nano-indentation load–displacement curves of (a) the 1140 °C/3 h sintered NiO + γ-alumina sample (NA1140A) and (b) the result after leaching by 50% NaOH solution for 80 min (NA1140B).

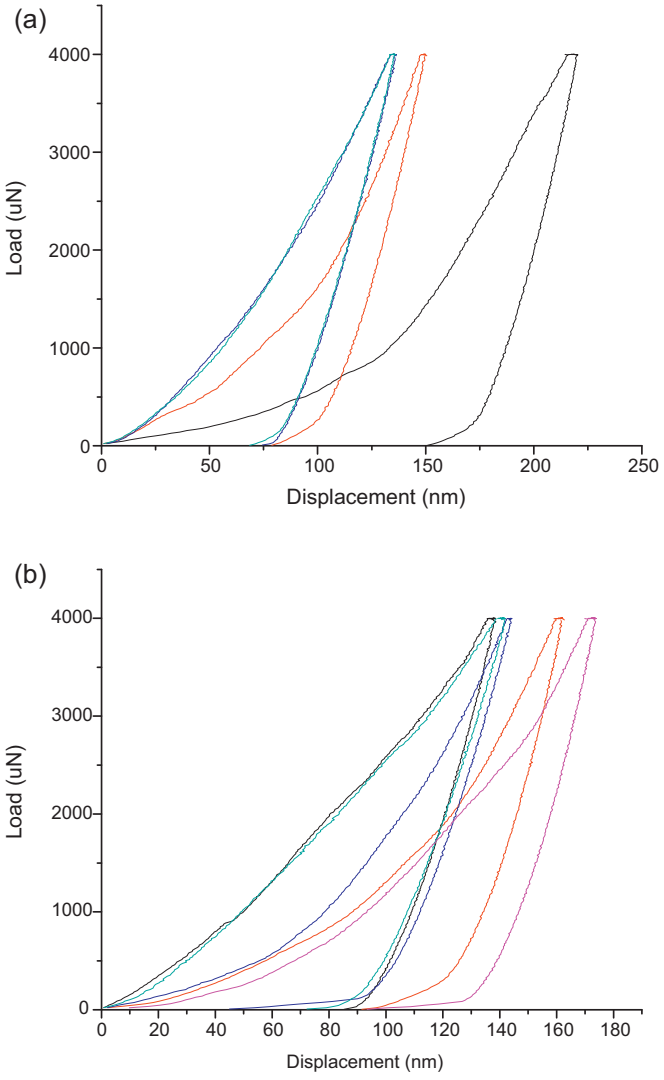

Fig. 7. Nano-indentation load–displacement curves of (a) the 1200 °C/3 h sintered NiO + γ-alumina sample (NA1200A) and (b) the result after leaching by 50% NaOH solution for 80 min (NA1200B).

Therefore, a sample with the same precursor (NiO + γ-Al_2O_3) was sintered at a slightly higher temperature (1200 °C) for nano-indentation experiments, aiming to explore whether a limited increase in temperature improves the mechanical properties. There was a noticeable increase in the mechanical properties of the sintered sample (NA1200A), with values of 4.5 GPa for nanohardness and 109.1 GPa for modulus, although the heterogeneous nature of the load–displacement curves was still observed due to the incomplete metal transformation reaction (Fig. 7a). These values are comparable to the property range of the cristobalite tested in the previous section, which plays a crucial role in the mechanical strength of clay-based ceramics. Moreover, it is evident that the spinel phase sintered at higher temperatures, such as 1480 °C, can further increase surface hardness and stiffness. The NA1200B sample was derived by leaching the NA1200A sample with a 50% NaOH solution for 80 min, and was then subject to nano-indentation experiments to generate the load–displacement curves shown in Fig. 7b. The nanohardness and modulus values estimated from the load–displacement curves were 7.1 GPa and 131.1 GPa respectively. This suggests that leaching the sample in an alkaline solution enhanced its mechanical property and improved its consistency, similar to the test for the sample sintered at 1140 °C. This repeated result clearly illustrates the adverse effect of intergranular substances and/or reactant residues among spinel grains when the processing temperature is insufficient to achieve a complete spinel formation and sintering effect. By removing these mechanically weaker materials with an alkaline solution, the overall nanohardness and modulus values on the material's surface are generally increased due to the stronger influence of the spinel.

4. Conclusion

The technological development of waste-to-resource strategies is important in both environmental and manufacturing industries. The incorporation of metal waste into the construction of ceramic products is viable due to the preferred stabilization mechanism of crystal structures and the large volume of ceramic products needed by the construction industry. However, because product safety and functionality should not be compromised, a fundamental understanding of the surface properties of metal containing phases should be further established, rather than relying solely on data from regulatory tests on bulk samples. The results of this study demonstrate the superior mechanical properties of nickel-containing spinel phase, compared with cristobalite silica matrix, even under severe acid attack. The nano-indentations on spinel samples sintered at low temperatures identified 1200 °C as the minimum temperature for the basic surface property of ceramics to develop. Acid and alkaline attacks do not weaken the nickel-incorporated spinel structure, which suggests an aluminate spinel phase is preferable for stabilizing the hazardous nickel ions in ceramic products.

Acknowledgments

This work was supported by Research Grants Council of Hong Kong (HKU 716310E) and Special Equipment Grant (SEG_HKU10) from University Grants Council of Hong Kong.

References

[1] C. Sandra, A. Roberta, L. Massimo, G. Alessandra, F. Pietro, S. Sergio, Soil genotoxicity assessment: a new strategy based on biomolecular tools and plant bioindicators, Environ. Sci. Technol. 36 (2002) 2748–2753.
[2] M. Nadal, M. Schuhmacher, J.L. Domingo, Metal pollution of soils and vegetation in an area with petrochemical industry, Sci. Total Environ. 321 (2004) 59–69.
[3] U. Farooq, J.A. Kozinski, M.A. Khan, M. Athar, Biosorption of heavy metal ions using wheat based biosorbents—a review of the recent literature, Bio. Technol. 101 (2010) 5043–5053.
[4] M. Alain, L. Kathryn, A. Nagy, L. Matthew, Marcus, Martine, Formation of metallic copper nanoparticles at the soil–root interface, Environ. Sci. Technol. 42 (2008) 1766–1772.
[5] T. Kozanecka, J. Chojnicki, W. Kwasowski, Content of heavy metals in plant from pollution-free regions, Pol. J. Environ. Stud. 11 (2002) 395–399.
[6] P.T. Bolger, D.C. Szlag, Investigation into the rejuvenation of spent electroless nickel baths by electrodialysis, Environ. Sci. Technol. 36 (2002) 2273–2278.
[7] R.W. Anderson, W.A. Neff, Electroless nickel bath recovery by cation-exchange and precipitation, Plat. Surf. Finish. 79 (1992) 18–26.
[8] F. Altmayer, T.D. Ferguson, J. Bridges, Nickel plating: industry practices control technologies and environmental management, USEPA Capsule Report 635/R-03/005, U.S. Government Printing Office, Washington, DC, 2003.
[9] S.R. Lim, J.M. Schoenung, Human health and ecological toxicity potentials due to heavy metal content in waste electronic devices with flat panel displays, J. Hazard. Mater. 177 (2010) 251–259.
[10] O. El Hamiani, H.E. Khalil, K. Lounate, C. Sirguey, M. Hafidi, G. Bitton, Toxicity assessment of garden soils in the vicinity of mining areas in Southern Morocco, J. Hazard. Mater. 177 (2010) 755–761.
[11] M. Pazos, G.M. Kirkelund, L.M. Ottosen, Electrodialytic treatment for metal removal from sewage sludge ash from fluidized bed combustion, J. Hazard. Mater. 176 (2010) 1073–1078.
[12] B.E. Tastan, S. Ertugrul, G. Donmez, Effective bioremoval of reactive dye and heavy metals by *Aspergillus versicolor*, BioTechnology 101 (2010) 870–876.
[13] B. Bayat, B. Sari, Comparative evaluation of microbial and chemical leaching processes for heavy metal removal from dewatered metal plating sludge, J. Hazard. Mater. 174 (2010) 763–769.
[14] C.-Y. Hu, K. Shih, J.O. Leckie, Formation of copper aluminate spinel and cuprous aluminate delafossite to thermally stabilize simulated copper-laden sludge, J. Hazard. Mater. 181 (2010) 399–404.
[15] Y. Tang, S.S.-Y. Chui, K. Shih, L. Zhang, Copper stabilization via spinel formation during the sintering of simulated copper-laden sludge with aluminum-rich ceramic precursors, Environ. Sci. Technol. 45 (2011) 3598–3604.
[16] K. Shih, T. White, J.O. Leckie, Nickel stabilization efficiency of aluminate and ferrite spinels and their leaching behavior, Environ. Sci. Technol. 40 (2006) 5520–5526.
[17] K. Shih, T. White, J.O. Leckie, Spinel formation for stabilizing simulated nickel-laden sludge with aluminum-rich ceramic precursors, Environ. Sci. Technol. 40 (2006) 5077–5083.
[18] E. Loginova, F. Cosandey, T.E. Madey, Nanoscopic nickel aluminate spinel ($NiAl_2O_4$) formation during NiAl [1 1 1) oxidation, Surf. Sci. 601 (2007) 11–14.
[19] K. Shih, J.O. Leckie, Nickel aluminate spinel formation during sintering of simulated Ni-laden sludge and kaolinite, J. Eur. Ceram. Soc. 27 (2007) 91–99.

[20] R.S. Zhou, R.L. Snyder, Structures and transformation mechanisms of η, γ and θ transition aluminas, Acta Crystallogr. Sect. B: Struct. Sci. 47 (1991) 617–630.
[21] B. Velde, Introduction to Clay Minerals, Chapman & Hall, London, 1992
[22] R.C. Bradt, D. Munz, M. Sakai, K.W. White, Fracture Mechanics of Ceramics, Springer, New York, 2003.
[23] R.A. Cutler, R.J. Mayhew, K.M. Prettyman, A.V. Virkar, High-toughness Ce-TZP/Al_2O_3 ceramics with improved hardness and strength, J. Am. Ceram. Soc. 74 (1991) 179–186.
[24] G. Fantozzi, G. Orange, K. Liang, M. Gautier, J.P. Duraud, P. Maire, Effect of nonstoichiometry on fracture toughness and hardness of yttrium oxide ceramics, J. Am. Ceram. Soc. 72 (1989) 1562–1563.
[25] R.W. Rice, C.C. Wu, F. Borchelt, Hardness–grain-size relations in ceramics, J. Am. Ceram. Soc. 77 (1994) 2539–2553.
[26] G.M. Pharr, W.C. Oliver, Nanoindentation of silver-relations between hardness and dislocation structure, J. Mater. Res. 4 (1989) 78–84.
[27] D.B. Sirdeshmukh, L. Sirdeshmukh, K.G. Subhadra, Micro-and Macro-properties of Solids, Springer, New York, 2006.
[28] G.M. Pharr, Measurement of mechanical properties by ultra-low load indentation, Mater. Sci. Eng. A 253 (1998) 151–159.
[29] C.A. Schuh, T.G. Nieh, A nanoindentation study of serrated flow in bulk metallic glasses, Acta Mater. 51 (2003) 87–99.
[30] Y. He, J.Z. Zhang, W.Q. Yao, D.Q. Li, X. Teng, Effect of temperature on residual stress and mechanical properties of Ti films prepared by both ion implantation and ion beam assisted deposition, J. Surf. Sci. 255 (2009) 4484–4490.
[31] Y. Wang, C. Suryanarayana, L. An, Phase transformation in nanometer-sized γ-alumina by mechanical milling, J. Am. Ceram. Soc. 88 (2005) 780–783.
[32] G.W. Brindley, M. Nakahira, The kaolinite–mullite reaction series. I. A survey of outstanding problems, J. Am. Ceram. Soc. 42 (1959) 311–314.
[33] G.W. Brindley, M. Nakahira, The kaolinite–mullite reaction series. II. Metakaolin, J. Am. Ceram. Soc. 42 (1959) 314–318.